Desalination and Water Treatment
www.deswater.com
doi: 10.5004/dwt.2021.26767

217 (2021) 101–110
March

Preparation and characterization of alumina hollow fiber membrane for oilfield produced water treatment

Sandriely Sonaly Lima Oliveira*, Rayssa de Almeida Àvila, Rodholfo da Silva Barbosa Ferreira, Vanessa da Nóbrega Medeiros, Edcleide Maria Araújo, Hélio de Lucena Lira

Membranes Development Laboratory, Federal University of Campina Grande, Campina Grande – Brazil, emails: sandriely_sonaly@hotmail.com (S.S.L. Oliveira), rayssaavila@hotmail.com (R. de Almeida Àvila), rodholfoferreira@gmail.com (R. da Silva Barbosa Ferreira), vanismedeiros@gmail.com (V. da Nóbrega Medeiros), edcleide.araujo@ufcg.edu.br (E.M. Araújo), helio.lira@ufcg.edu.br (H. de Lucena Lira)

Received 4 June 2020; Accepted 5 November 2020

ABSTRACT

Currently one of the greatest challenges of humanity is the preservation of the environment, especially in relation to natural water sources. An efficient way to treat aqueous effluents is with the use of the membranes separation process. At present ceramic hollow fiber membrane has been extensively explored and fabricated via extrusion. In this study, the alumina hollow fiber membrane was fabricated through the phase inversion technique, with variations in sintering temperature, composition and processing parameters to verify the efficiency of membranes in effluent treatment. Morphological investigation revealed that the membranes had an asymmetric structure even after the sintering process. Porosity decreased inversely proportionally as the firing rate increased, the membranes presented porosity above 30%. In addition, due to the sintering temperature, the mechanical resistance reached 35 MPa. The membranes manufactured in this study have a broad potential to be applied in oil–water separation with an efficiency above 90%.

Keywords: Membranes; Hollow fiber; Alumina; Phase inversion; Sintering

1. Introduction

In recent years membranes have shown their potential for rationalization water separation and treatment systems, as they do not require the use of chemicals, operate at room temperature, are relatively easy to use and in some cases, and may be applied in the separation of mixtures of liquids and gases [1,2].

The factors that determine the viability in a membrane system is the degree of separation obtained in the process and the lifetime of the membrane, which are dependent on the properties of the materials that make up the membranes. In many cases, the lifetime of these membranes can make processes economically unfeasible, however, ceramic membranes have contributed to reduce this problem, mainly due to several features that are associated with their properties [3–5].

The mechanical and selectivity properties of membranes and the driving force involved in transporting through membranes depend on the apparent porosity, distribution and size of pores, which are mainly determined by the starting materials, sintering processes and manufacturing methods [6].

There are several techniques of producing membranes, however, phase inversion is the most used method in obtaining polymeric membranes, mainly in the form of hollow fibers, which are produced by the precipitation of an extruded solution, and subsequent precipitation in a

* Corresponding author.

non-solvent bath. The membrane is formed by the destabilization of the solution and precipitation of the polymer. This technique allows extensive morphological modification from small variations made in the parameters used during the membrane preparation process [7–9]. Because it is a relatively simple procedure, more than 80% of the membranes produced on the market are prepared by this technique [10]. Membranes with hollow fiber geometry allow the obtaining of a membrane with a small diameter (0.1–1 mm) [11] allowing a large membrane area per unit volume, easy to manufacture module and high-density packaging [12].

Alumina was chosen in this study as materials to compose the membranes because of its present excellent mechanical properties, high packaging density, uniformity of particle size distribution and chemical stability [9,13–15]. Alumina membranes can be easily applied in the separation of liquid and gas at high temperatures, which make them tolerate more severe operating conditions, and greater resistance to higher pressures, increasing the efficiency of separation processes [16].

Most alumina ceramic membranes used in wastewater treatment are not fibers [17]. The interest in developing alumina hollow fiber membranes grew rapidly after a successful preparation of polymer hollow fiber membrane and apparently crack-free molecular sieving hollow fiber membranes by carbonizing cellulose hollow fiber [18]. Therefore, it is necessary to investigate the processing variables to prepare hollow fiber ceramic membranes with adequate morphology and properties, since the morphological characteristics of the membranes play a fundamental role in the treatment performance.

This work aims to prepare alumina hollow fiber membrane, to investigate how the sintering temperature and spinning parameters affect the membrane property and additionally to evaluate the separation performance in the treatment of oily wastewater emulsion.

2. Materials and methods

2.1. Materials

For the development of the research, the following materials were used: calcined alumina (Al_2O_3), provided by Imerys Fused Minerals (Villach, Austria), with high purity (>99.8%), particle size (d_{50} = 2.0 μm) and relatively monodispersed (0.3–3.9 μm). Polyethersulfone (PES), with the trade name of Veradel® 3000P, supplied by Solvay (Brussels, Belgium) and used as a polymer matrix. N,N-Dimethylformamide p.a., ACS (DMF), from Neon Comercial Ltd (São Paulo, Brazil), used as a solvent to dissolve the polymer and additives. Polyvinylpyrrolidone (PVP) $(C_6H_9NO)_n$, produced by Labsynth Produtos para Laboratórios Ltd (São Paulo, Brazil) is used as a viscosifying additive.

2.2. Methods

Initially, PES was dried at 80°C for 24 h to eliminate adsorbed water. For the preparation of the suspension PES, PVP and DMF were mixed in a mechanical agitator at 1,000 rpm for 60 min, then added the alumina and remained stirring for another 30 min at 1,000 rpm. After mixing, the suspension was screened through a 110 mesh sieve and remained at rest for 24 h, for stabilization and elimination of possible bubbles.

The membranes were obtained from the compositions in Table 1. The ceramic suspensions with different alumina contents were investigated and resulted in an adequate viscosity to obtain the hollow fiber configuration during the extrusion-based on process phase inversion. The concentration of alumina was increased from 56 to 59 wt.% to obtain a homogeneous dispersion with the proportion of one part of PES to five parts of alumina. It should be noted that PES concentration should be equal to or more than 5 wt.% to enable hollow fiber spinning by the phase inversion technique and to prevent it from affecting the inversion capability.

The processing conditions are shown in Table 2. The flow rate of the bore liquid (distilled water) was kept fixed at 400 mL/h with the aid of a SP900Vet syringe pump, from the Centaurus Medical brand (Amsterdam). Viscosity measurements were performed at room temperature, using the Quimis Q860M21 Rotary Viscometer, with a reading range of 100 to 600,000 mPa·s.

For membrane preparation, the phase inversion method was used through the immersion-precipitation technique, in Fig. 1. The suspension was placed in an extruder to produce hollow fiber membranes by precipitation in a distilled water bath.

The membranes were sintered in a conventional electric oven from Maitec Fornos INTI (São Carlos, Brazil), with maximum temperatures of 1,400°C and 1,500°C, a heating rate of 2°C/min and burning level of 1 h at the maximum temperature. After the heat treatment, the fibers were cut in a length of 5 cm, for the assembly of the modules.

Table 1
Compositions of suspensions C1 and C2

Compositions	C1	C2
Al_2O_3 (%)	56	59
Polyethersulfone (%)	5	6
N,N-Dimethylformamide (%)	38	34
Polyvinylpyrrolidone (%)	1	1

Table 2
Parameters for preparing alumina hollow fiber membranes

Parameters	Value
Internal liquid	H_2O
Precipitation bath	H_2O
Pressure	1 and 3 bar
Air gap	0, 5 and 10 cm
Dope flow rate	400 mL/h
Bore fluid flow rate	400 mL/h
Suspension viscosity C1	1,038.9 mPa·s
Suspension viscosity C2	6,351.8 mPa·s
External extruder diameter (mm)	2.35 mm
Internal extruder diameter (mm)	1.17 mm

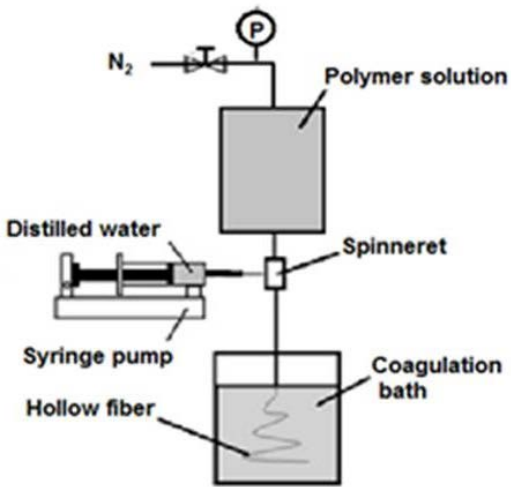

Fig. 1. Schematic representation of the extruder to produce hollow fiber membranes. Adapted based on the study of Luiten-Olieman et al. [19].

The raw materials were characterized by laser diffraction (granulometry) from Mastersizer brand Malvern instruments, model 2000, X-ray diffraction (Shimadzu XDR-6000 (Kyoto, Japan), using Cukα radiation (λ = 1.5418 Å), the voltage of 40 kV, 30 mA current, scan range 2θ from 5° to 80° and scan speed of 2°/min). The membranes were characterized by scanning electron microscopy (SEM; Superscan SSX-550 – Shimadzu, operating at 15 kV).

The porosity of the membranes was evaluated by the apparent porosity (PA), which is defined as the volumetric percentage of open porosity in the sample. Its measurement was made by the Archimedes gravimetric method, following Eq. (1).

$$\mathrm{PA} = \left(\frac{P_U - P_S}{P_U - P_I}\right) \times 100(\%) \tag{1}$$

where P_S is the weight of the dry sample, P_U is the weight of the wet sample and P_I is the weight of the sample when immersed in water. It was used at least 10 samples to calculate the standard deviation.

The mechanical strength of the fibers was examined by a three-point bending test using the EMIC machine (São José dos Pinhais, Brazil) equipped with a 1 kN load cell. The flexural strength (σ_F) of each fiber was calculated using Eq. (2) [20], was used ten hollow fiber membranes to calculate the average value:

$$\sigma_F = \frac{8FL\mathrm{Do}}{\pi\left(\mathrm{Do}^4 - \mathrm{Di}^4\right)} \tag{2}$$

where F is the force at which the fracture occurred (N). L, Do, and Di are the length (m), the outer and inner diameter (m) of the hollow fiber, respectively.

The permeate flow analysis was performed with distilled water at 25°C, in a laboratory system with the tangential flow, using pressures of 0.5 and 1.0 bar.

The calculation of the volumetric flow (J) collected for all membranes was calculated using Eq. (3).

$$J = \frac{\text{Permeated volume}\left(\mathrm{L}\right)}{\text{Membrane area}\left(\mathrm{m}^2\right) \times \text{Time}\left(\mathrm{h}\right)} \tag{3}$$

Emulsion with 250 ppm of oil (crude oil) was prepared with the aid of a stirrer model Ultra Turrax® T18 basic from IKA Works Inc. (Kuala Lumpur, Asia) with a speed of 15,000 rpm, for a period of 30 min. The transmembrane pressure was kept constant at 1 bar. The oil concentrations present in the permeate samples were measured using the BEL Photonics spectrophotometer, (Monza, Italy) (UV-Vis), model UV-M51. Eq. (4) was used to evaluate oil rejection:

$$\text{Rejection} = \frac{A_i - A_0}{A_i} \times 100(\%) \tag{4}$$

where A_i is the concentration of the oil in the feed and A_0 are the concentrations of the oil in the permeate.

3. Results and discussion

3.1. Particle size distribution

Fig. 2 shows the particle size distribution of the alumina powder. It is observed that the alumina presented a narrow range for the distribution of the diameter, with an average value of 2.03 μm. The narrower the distribution is shown by the particle diameter curve, the greater the homogeneity in terms of the distribution, size and geometry of the membrane pores [21]. Table 3 shows the distribution values.

3.2. X-ray diffraction

Fig. 3 illustrates the results of X-ray diffraction of membranes after sintering at 1,500°C. It is clear the presence of α-alumina (standard card PDF 10-0173), after sintering at temperatures greater than approximately 800°C all the other components from the ceramic suspension was eliminated. Despite the difference in composition and

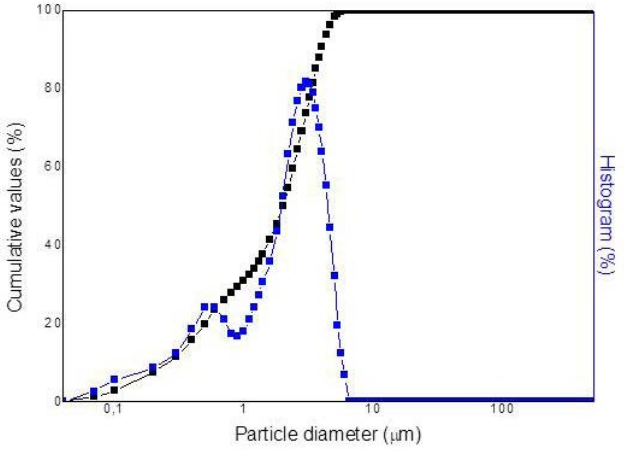

Fig. 2. Granulometric distribution of alumina.

Table 3
Values of particle size distribution

D10 (μm)	0.26
D50 (μm)	2.01
D90 (μm)	3.96
Dm (μm)	2.03

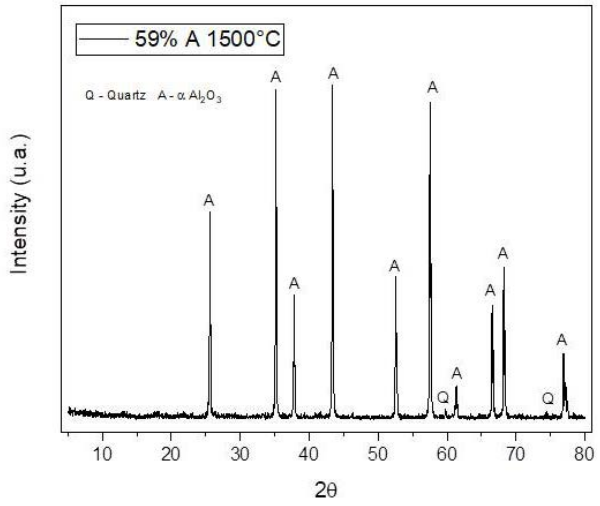

Fig. 3. X-ray diffraction of membranes after sintering at 1,500°C.

sintering temperature, there is no change in the phase constituents. Alumina in its alpha polymorphic form (α) presents high stability and resistance to harsh environments (high acidity or alkalinity) making this material important in the production of ceramic membranes [9,14,22–25].

3.3. Scanning electron microscopy

The images of the membranes obtained by SEM with 56% and 59% of alumina can be seen in Figs. 4 and 5, respectively, where they were taken in the cross-section of the membranes after sintering, in order to verify the influence of the gap used in their morphology.

In general, the cross-section of the membranes is porous and asymmetrical. These spongy structures present in hollow alumina fiber membranes were caused by the precipitation of the polymeric phase during the phase inversion process [25].

For all regions of the cross-section, the pores remained internally interconnected, which can be attributed to the polymer leaving after burning [26]. The increase in the sintering temperature did not cause significant changes in the morphology of the membranes.

The change in the morphology of the ceramic membranes is due to the variation of the air gap used during the spinning process. As the air gap increased, the diameters of the membrane decreased. This behavior is related to the fact that, during the interval in which the fiber is exposed to air, there is elongation stress in the fibers before their complete precipitation by immersion in the bath. This reduction in wall thickness will influence the permeability of the membrane [7,27]. According to Chung et al. [28], high stress of elongation can pull the molecular chains or separate phases and increase porosity, while medium stress can induce molecular orientation and reduce the porosity of the membrane or free volume. The membranes obtained with 56% alumina and sintered at 1,400°C and 1,500°C have a sandwich-like structure, with macro-voids structures from the inner and outer surface of the ceramic hollow fiber membrane. The appearance of these pores may be related to the viscosity of the dispersion and linked to the increase in the porosity and permeability of these samples, the lower the viscosity the greater the tendency to form macro-voids. The membranes with 56% of alumina showed a viscosity six times lower when compared to the membranes with 59% of alumina. Lee et al. [29] explained that the energy responsible for the flow of the internal liquid (water) in the ceramic dispersion is dissipated during micro-void formations due to the viscosity of the ceramic dispersion. During the phase inversion process, the viscosity of the ceramic dispersion is increased as the solvent/non-solvent exchange occurs, and the formation of micro-voids throughout the membrane structure is inhibited. This was observed in the middle layer of the membrane, characterized by a sponge-like region. With the increase in sintering temperature, it is possible to observe that this middle layer becomes more evident, as well as the macro-voids.

Based on Fig. 5, it was found that there is no presence of large "fingers" in the transversal of the SEM image of the membranes with 59% alumina. The structure remained porous, with reduced thickness, resulting from the contraction mechanism.

The wall thickness and average pore size of alumina hollow fiber membranes produced with different air-gap are shown in Table 4.

With the increase in alumina content, it was possible to observe a decrease in pore size, which is related to the solids content in the dispersion and after sintering greater compaction can be observed. According to Table 4, the pore size of the membranes decreased with the increase in the sintering temperature, ranging from 10–20 μm. Pore sizes are in an appropriate pore size range for microfiltration applications [19].

3.4. Apparent porosity

According to Fig. 6, the porosity of the sintered ceramic membranes at different temperatures is between 30% and 41% and, the increase in the sintering temperature caused the porosity to decrease [29].

It is possible to notice that with the increase of the air gap, during fiber processing, there is a slight increase in the porosity of the membranes, due to the time of exposure to air and, consequently, their precipitation and the appearance of pores. In general, membranes with 56% burned at 1,400°C and 1500°C showed higher porosity values. This can be related to the SEM images (the pores in the shape of macro-voids most visible in these compositions) and to a lesser amount of alumina.

It should be mentioned that all porosity values are above 30%. Honda et al. [30] stated that to minimize the

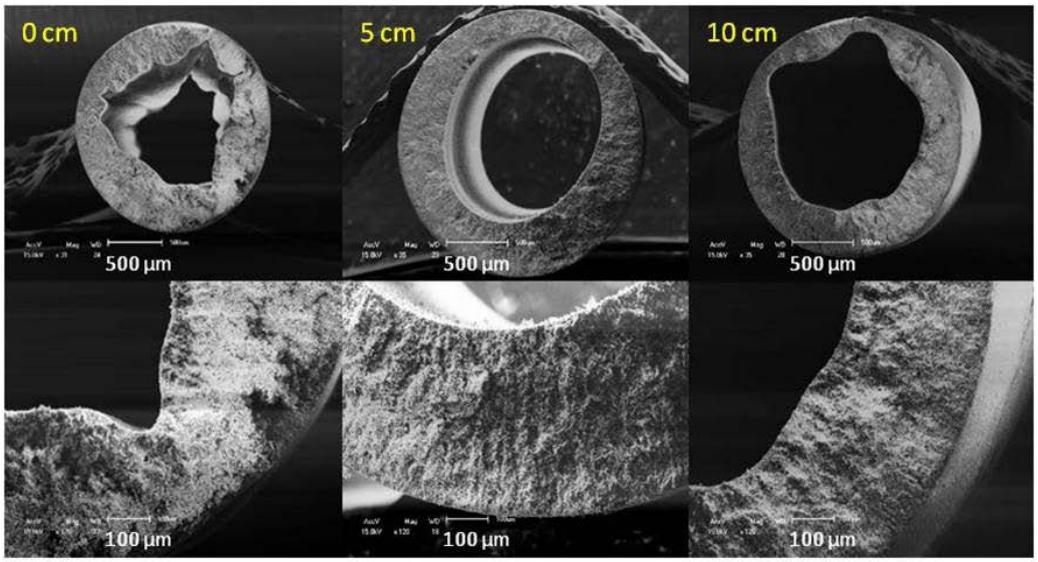

(a)

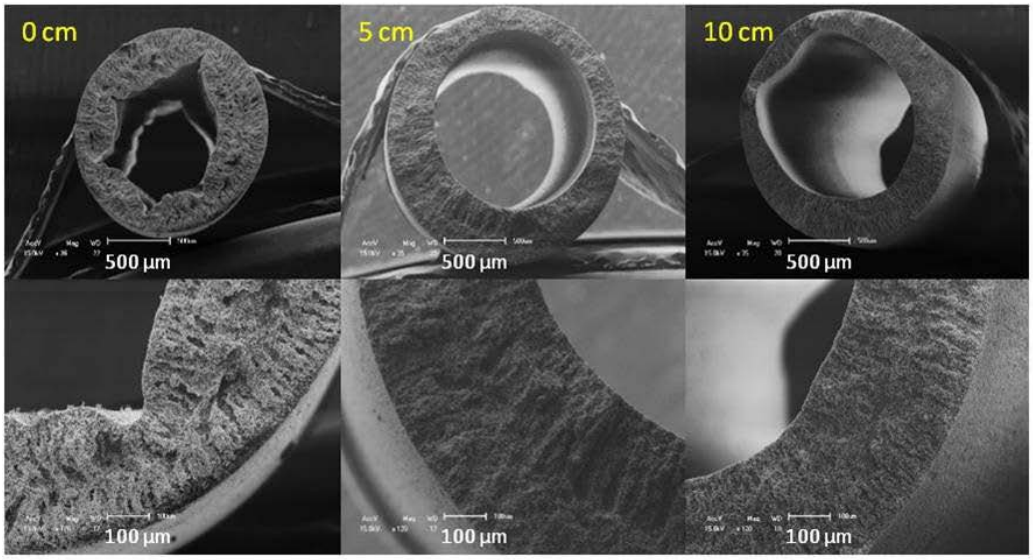

(b)

Fig. 4. Scanning electron microscopy images of the ceramic membrane with 56% alumina, sintered at 1,400°C (a) and 1,500°C (b) with a gap of 0, 5 and 10 cm and magnification of 35× and 120×, respectively.

pressure drop, porous ceramic membranes should have a relatively higher porosity, above 30%. Therefore, it can be concluded that there is enough porosity for the ceramic membranes obtained in this study to be applied in the separation process.

3.5. Mechanical resistance

The mechanical resistance of the membranes with different alumina contents is shown in Fig. 7. The sintering temperature affected the mechanical characteristics of the alumina membranes. As the sintering temperature increased, the alumina particles packed more densely, which increased the mechanical strength and decreased the pore size. For separation applications, a hollow fiber membrane with higher mechanical strength has better self-supporting capacity and a better backwash performance [31]. It was observed that the mechanical strength of the fibers reached a value of 35 MPa for the sintering temperature of 1,500°C with 59% alumina and with a gap of 0 cm.

It is possible to observe that the higher the alumina content, the greater the mechanical strength; and the greater the air gap, the lower the resistance.

3.6. Water flow measurements

Flow measurements with distilled water were performed at pressures of 0.5 and 1.0 bar. Figs. 8 and 9 illustrate the

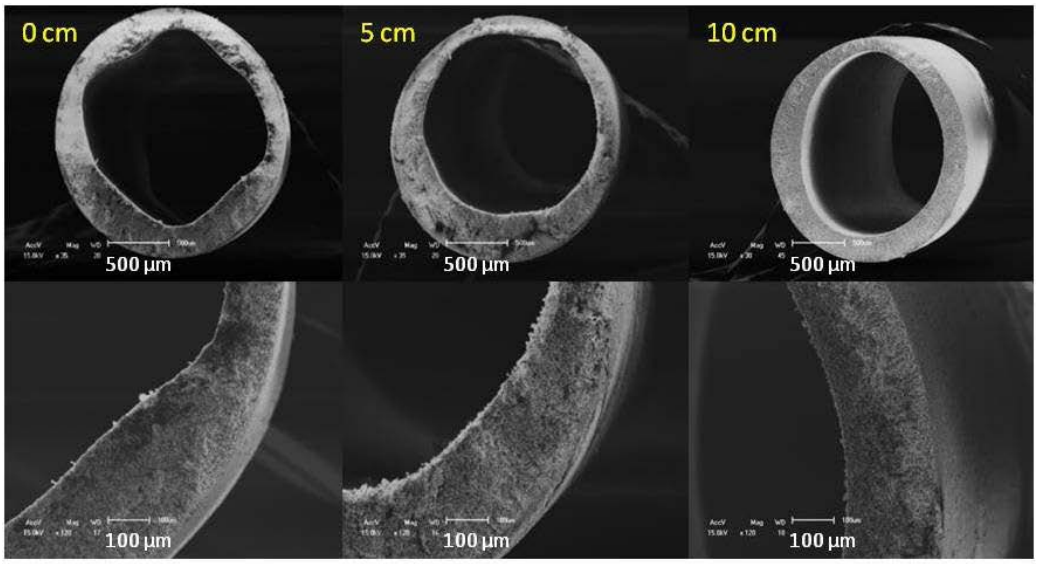

(a)

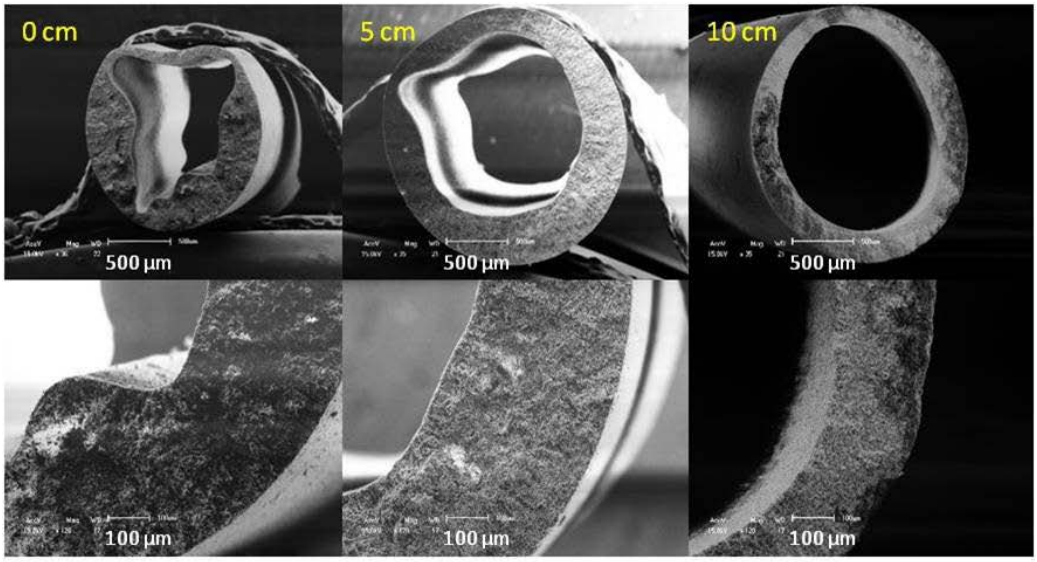

(b)

Fig. 5. Scanning electron microscopy images of the ceramic membrane with 59% alumina, sintered at 1,400°C (a) and 1,500°C (b) with a gap of 0, 5 and 10 cm and magnification of 35× and 120×, respectively.

permeated flow with distilled water through the membranes with 56% and 59% alumina, respectively.

For membranes with 56% alumina–10 cm–1,400°C the initial flow was 2,596 L/h m^2 with 0.5 bar pressure and decreased significantly to 714 L/h m^2 after 1 h of testing, the one with the best permeation. According to Elmaleh and Naceur [32], the decrease is due to clogging by microparticles, probable microorganisms with a size between 1 and 10 µm which can develop in the tank even if the initial water is of high purity. To Hubadillah et al. [33], the decrement of water flux over time is due to the stability of water permeate through the membrane pores. The water particles easily pass through the membrane pores. After some time, the pores have been filled with water by the monolayer formation by adsorption of water molecules followed by the condensation of water molecules within the pores and the flow of water flux through the membrane is starting to stablize.

The increase in the sintering temperature also caused a decrease in the permeate flow, due to the reduction of membrane porosity caused by the densification process. The increase in the gap caused an increase in the values of permeated water flow, which is related to a lower thickness of the membrane walls and a slight increase in porosity. The same behavior was observed by Lee et al. [34], Abdullah et al. [35] and Honda et al. [30]. The membranes with the

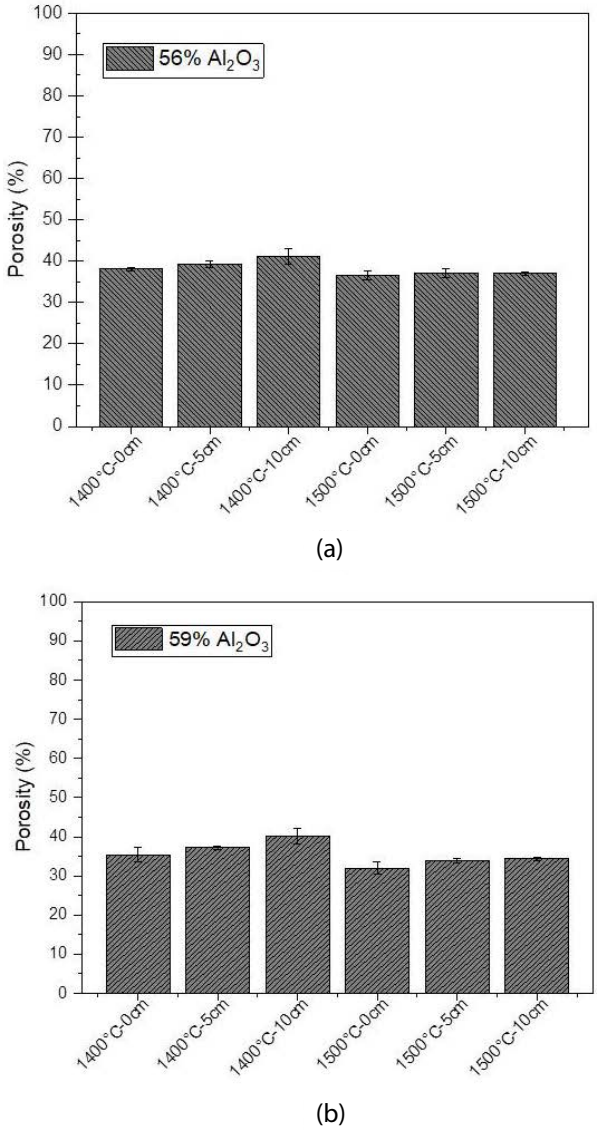

Fig. 6. Porosity of membranes with 56% (a) and 59% alumina (b).

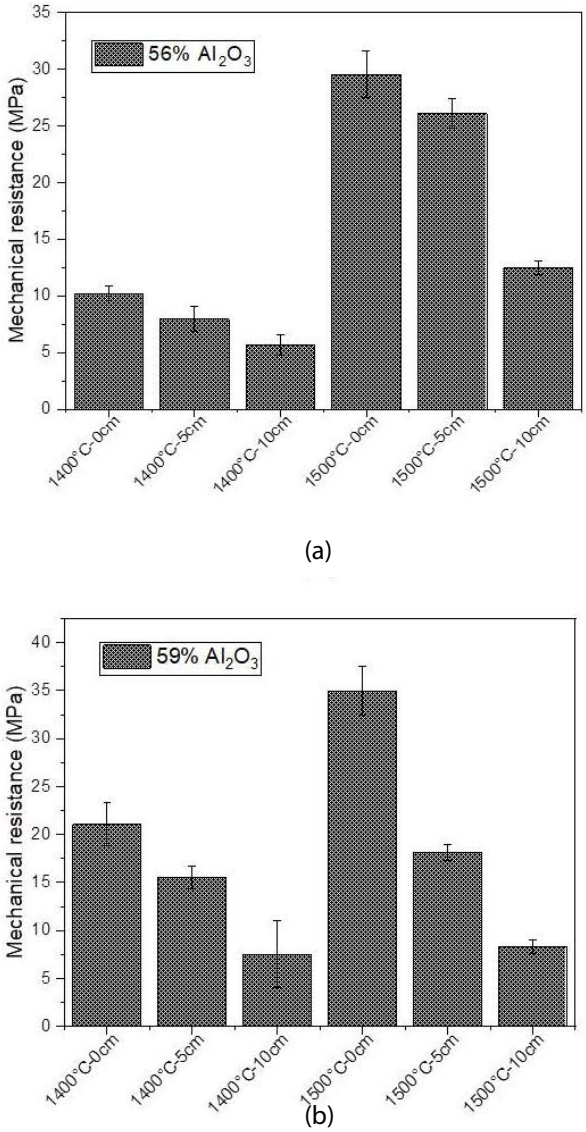

Fig. 7. Mechanical resistance of hollow fiber membranes with 56% (a) and 59% alumina (b).

lower sintering temperature and higher air gap showed higher flows due to the higher porosity of these membranes.

3.7. Separation of water–oil emulsion by membranes

The permeate flow with oil–water emulsion (Figs. 10 and 11) showed a behavior with high initial values of 2,100 L/h m^2 for the membrane of 0 cm gap and 1,400°C, and 700 L/h m^2 for the membrane of 0 cm and 1,500°C, reaching stability after 20 min. This decrease in permeate flow can be attributed, according to Abadi et al. [36], to the hydration of the membranes with water from the emulsion, and to the formation of oil incrustations on the membrane surface.

As well as this drop in flux is likely to be due to the concentration polarization effect, which is caused by the formation of an organic and inorganic fouling layer on the surface of the alumina composite hollow fiber membranes as oil concentration in the feed solution increases with time [37]. It can be observed that there was a reduction in flow with the increase of the air gap, which is associated with the size of pores. With a smaller pore size, a layer of oil is formed on the surface of the membrane, thus reducing the permeate flow.

Through the images by OM-LEICA DM750 (Wetzlar, Germany) (Fig. 12), it was possible to calculate the average size of the oil droplets, which was 6.25 μm. The rejection values of membranes for oil–water emulsion separation, with a feed concentration of 250 ppm, are shown in Table 5.

All membranes showed oil rejection above 90%. With the increase in temperature, as well as the alumina content, there was an increase in oil rejection, which is associated with reduced porosity. On the other hand, the increase in the gap caused a reduction in this efficiency, associated with the greater porosity.

Table 4
Wall thickness and pore size of the asymmetric alumina hollow fiber membranes

Composition 1			Composition 2		
C1	Wall thickness (mm)	Mean pore size (μm)	C2	Thickness (mm)	Mean pore size (μm)
56%–0 cm–1,400°C	0.40	20.45	59%–0 cm–1,400°C	0.33	18.12
56%–5 cm–1,400°C	0.36	17.71	59%–5 cm–1,400°C	0.31	15.78
56%–10 cm–1,400°C	0.31	12.93	59%–10 cm–1,400°C	0.27	10.31
56%–0 cm–1,500°C	0.37	19.47	59%–0 cm–1,500°C	0.42	13.36
56%–5 cm–1,500°C	0.34	11.71	59%–5 cm–1,500°C	0.33	11.04
56%–10 cm–1,500°C	0.29	10.36	59%–10 cm–1,500°C	0.25	10.02

Calculation based on ImageJ.

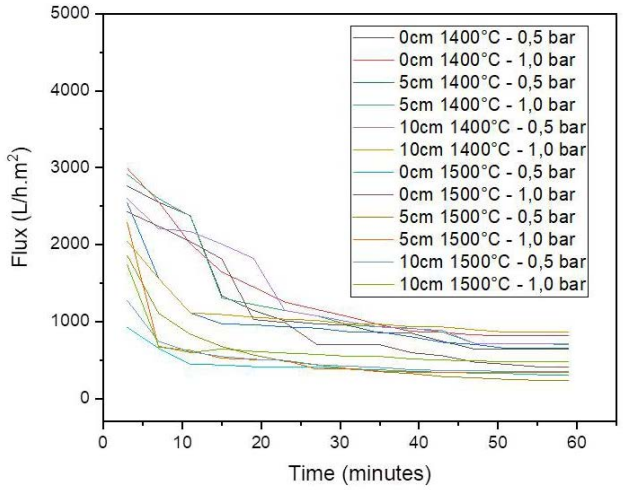

Fig. 8. Flow permeated with water distilled through the membrane with 56% of alumina, gap of 0, 5 and 10 cm, sintered at 1,400°C and 1,500°C, respectively, at pressures of 0.5 and 1.0 bar.

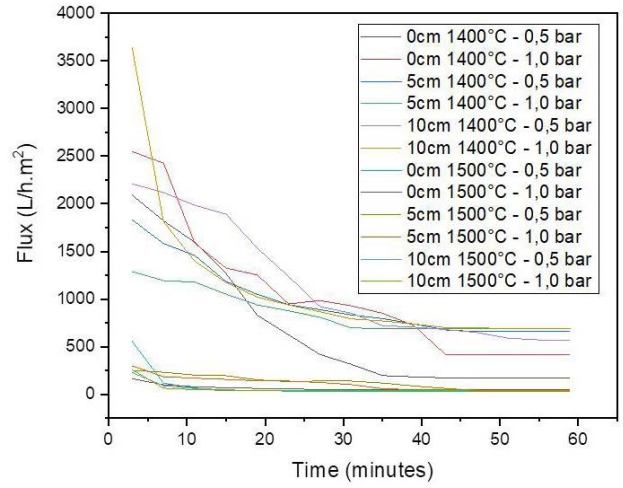

Fig. 9. Flow permeated with distilled water through the membrane with 59% of alumina with a gap of 0, 5 and 10 cm, sintered at 1,400°C and 1,500°C respectively, at pressures of 0.5 and 1.0 bar.

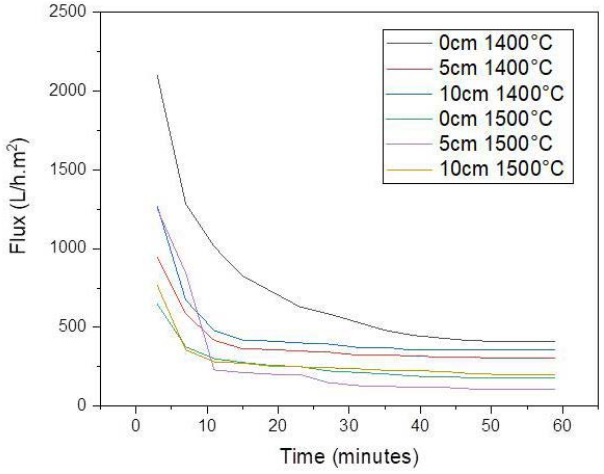

Fig. 10. Flow permeated with oil–water emulsion by the membrane of 56% alumina, gap of 0, 5 and 10 cm and sintered at 1,400°C and 1,500°C, respectively, at a pressure of 1.0 bar.

Table 5
Rejection values of the oil–water emulsion under study

Composition	56% of Al_2O_3	59% of Al_2O_3
0 cm–1,400°C	93.2%	95.8%
5 cm–1,400°C	91.1%	93.4%
10 cm–1,400°C	90.5%	91.6%
0 cm–1,500°C	94.3%	97.8%
5 cm–1,500°C	92.5%	95.3%
10 cm–1,500°C	91.6%	93.5%

Fig. 13 shows images with images of an emulsion of water–oil used in the feed and permeated collected after separation with the membrane of 59% alumina–0cm–1,500°C. The permeate (Fig. 13b) did not present any macroscopically suspended particles when compared to the emulsion used in the feed (Fig. 13a). This indicates that the membrane shows a high potential for application in the wastewater treatment of the petrochemical industry.

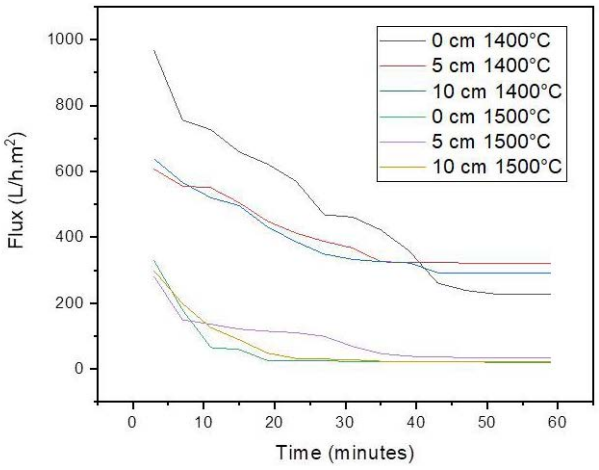

Fig. 11. Flow permeated with water–oil emulsion by the membrane of 59% of alumina, gap of 0, 5 and 10 cm and sintered at 1,400°C and 1,500°C, respectively, at a pressure of 1.0 bar.

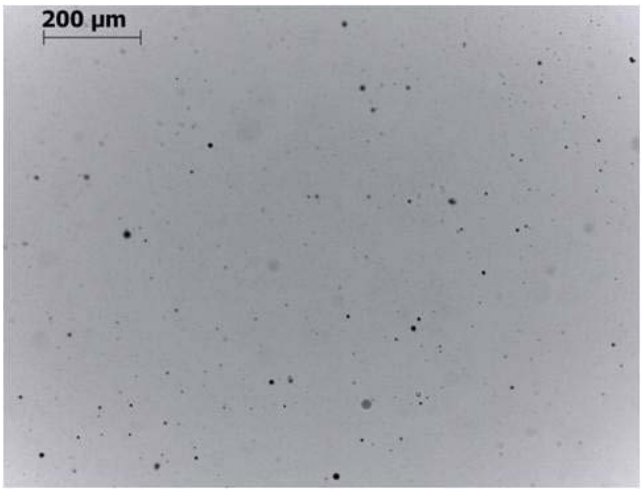

Fig. 12. Micrograph obtained by optical microscopy of the water–oil emulsion.

4. Conclusions

Membranes with 56% and 59% of alumina were successfully obtained through the phase inversion method and sintering at temperatures of 1,400°C and 1,500°C. The change in the alumina content, as well as in the extrusion parameters, influenced the characteristics of the formed membranes, causing changes in the viscosity of the ceramic suspension, in the morphology, mechanical properties, porosity and permeability of the hollow fiber ceramic membranes. The variation of the air gap changed the morphology of the membranes, the greater the gap the smaller the thickness of the membranes, the lower the mechanical resistance and the greater the flow. The increase in temperature caused a greater sintering of the alumina grains, increasing the density and mechanical resistance and decreasing the size of the pores. The increase in sintering temperature from 1,400°C to 1,500°C reduced the permeate flow of distilled water from 714 L/h m^2 to value of

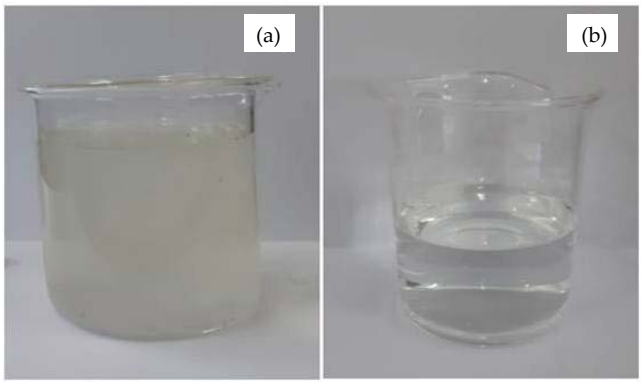

Fig. 13. Images of the emulsion of water–oil used in the feed (a) and permeated collected (b) after separation with the membrane of 59% alumina-0 cm–1,500°C.

235.60 L/h m^2. For oil–water emulsion separation, the flows of the alumina membranes dropped to values of 400 L/h m^2 and showed 97% oil rejection, demonstrating the potential of these membranes for treatment of effluents.

Acknowledgment

The authors would like to acknowledge the CNPq, CAPES for financial support, and Federal University of Campina Grande for the technical support.

References

[1] M.F. Zawrah, R.M. Khattab, L.G. Girgis, E.E. El Shereefy, S.E. Abo Sawan, Effect of CTAB as a foaming agent on the properties of alumina ceramic membranes, Ceram. Int., 40 (2014) 5299–5305.
[2] H. Strathmann, L. Giorno, E. Drioli, An Introduction to Membrane Science and Technology, Wiley-VCH, Weinheim, 2011.
[3] A.C. Habert, C.P. Borges, R. Nóbrega, Processos de separação com membranas, E-papers Serviços Editoriais, Rio de Janeiro, 2006.
[4] M.M. Viana, V.F. Soares, N.D.S. Mohallem, Synthesis and characterization of TiO_2 nanoparticles, Ceram. Int., 36 (2010) 2047–2053.
[5] A.C. Chaves, H.L. Lira, G.A. Neves, F.A. Silva, R.C.O. Lima, K.B. França, Preparation and characterization of tubular ceramic membranes using mass incorporated with clay, kaolin and quartz, Cerâmica, 59 (2013) 192–197.
[6] X.-L. Guo, M. Huang, J. Yan, S. Li, K. Wang, R. Si, C.-Y. Chen, Correlation effects on the fine-structure splitting within the $3d^9$ ground configuration in highly-charged Co-like ions, Chin. Phys. B, 25 (2015) 013101.
[7] Z.T. Wu, R. Faiz, T. Li, B.F.K. Kingsbury, K. Li, A controlled sintering process for more permeable ceramic hollow fibre membranes, J. Membr. Sci., 446 (2013) 286–293.
[8] P. Anadão, Ciência e Tecnologia de Membranas, Artliber Editora, São Paulo, 2010.
[9] P. de Wit, F.S. van Daalen, N.E. Benes, The effect of the production method on the mechanical strength of an alumina porous hollow fiber, J. Eur. Ceram. Soc., 37 (2017) 3453–3459.
[10] N.N. Li, A.G. Fane, W.S.W. Ho, T. Matsuura, Advanced Membrane Technology and Applications, A John Wiley & Sons Inc., United States, 2008.
[11] A.F. Ismail, K.C. Khulbe, T. Matsuura, RO Membrane Fouling, Reverse Osmosis, Elsevier, Amsterdam, 2019.

[12] L. Luo, P. Wang, S. Zhang, G. Han, T.-S. Chung, Novel thin-film composite tri-bore hollow fiber membrane fabrication for forward osmosis, J. Membr. Sci., 461 (2014) 28–38.
[13] M.B. Thürmer, P. Poletto, M. Marcolin, J. Duarte, M. Zeni, Effect of non-solvents used in the coagulation bath on morphology of PVDF membranes, Mater. Res., 15 (2012) 884–890.
[14] I.-H. Choi, I.-C. Kim, B.-R. Min, K.-H. Lee, Preparation and characterization of ultrathin alumina hollow fiber microfiltration membrane, Desalination, 193 (2006) 256–259.
[15] L.L. Li, M.L. Chen, Y.C. Dong, X.F. Dong, S. Cerneaux, S. Hampshire, J.J. Cao, L. Zhu, Z.W. Zhu, J. Liu, A low-cost alumina-mullite composite hollow fiber ceramic membrane fabricated via phase-inversion and sintering method, J. Eur. Ceram. Soc., 36 (2016) 2057–2066.
[16] E. Salehi, S.S. Madaeni, A.A. Shamsabadi, S. Laki, Applicability of ceramic membrane filters in pretreatment of coke-contaminated petrochemical wastewater: economic feasibility study, Ceram. Int., 40 (2014) 4805–4810.
[17] M. Lee, Z. Wu, K. Li, Advances in Ceramic Membranes for Water Treatment, Advances in Membrane Technologies for Water Treatment, Woodhead Publishing, Oxford, 2015.
[18] A.F. Ismail, K. Li, From polymeric precursors to hollow fiber carbon and ceramic membranes, Membr. Sci. Technol., 13 (2008) 81–119.
[19] M.W.J. Luiten-Olieman, L. Winnubst, A. Nijmeijer, M. Wessling, N.E. Benes, Porous stainless steel hollow fiber membranes via dry–wet spinning, J. Membr. Sci., 370 (2011) 124–130.
[20] Y.-L.E. Fung, H.T. Wang, Nickel aluminate spinel reinforced ceramic hollow fibre membrane, J. Membr. Sci., 450 (2014) 418–424.
[21] M.C. da Silva, H.L. Lira, N.L. de Freitas, Asymmetric ceramic membrane based on clay for application in microfiltration process: influence of time of deposition, Cerâmica, 60 (2014) 436–442.
[22] J.E. Gardolinski, H.P. Martins Filho, F. Wypych, Thermal behavior of hydrated kaolinite, Quim. Nova, 26 (2003) 30–35.
[23] S.G. Medeiros, R.P.S. Dutra, J.P.F. Grilo, A.E. Martinelli, C.A. Paskocimas, D.A. Macedo, Preparation of low-cost alumina-mullite composites via reactive sintering between a kaolinite clay from Paraíba and aluminum hydroxide, Cerâmica, 62 (2016) 266–271.
[24] F. Sahnoune, M. Chegaar, N. Saheb, P. Goeuriot, F. Valdivieso, Algerian kaolinite used for mullite formation, Appl. Clay Sci., 38 (2008) 304–310.
[25] N. Abdullah, M.A. Rahman, M.H.D. Othman, J. Jaafar, A.A. Aziz, Preparation, characterizations and performance evaluations of alumina hollow fiber membrane incorporated with UiO-66 particles for humic acid removal, J. Membr. Sci., 563 (2018) 162–174.
[26] A.M.D. Leite, L.F. Maia, R.A. Paz, E.M. Araújo, H.L. Lira, Thermal properties from membrane of polyamide 6/montmorillonite clay nanocomposites obtained by immersion precipitation method, J. Therm. Anal. Calorim., 97 (2009) 577–580.
[27] W.X. Deng, X.H. Yu, M. Sahimi, T.T. Tsotsis, Highly permeable porous silicon carbide support tubes for the preparation of nanoporous inorganic membranes, J. Membr. Sci., 451 (2014) 192–204.
[28] T.S. Chung, S.K. Teoh, X.D. Hu, Formation of ultrathin high-performance polyethersulfone hollow-fiber membranes, J. Membr. Sci., 133 (1997) 161–175.
[29] M. Lee, Z.T. Wu, R. Wang, K. Li, Micro-structured alumina hollow fibre membranes – potential applications in wastewater treatment, J. Membr. Sci., 461 (2014) 39–48.
[30] S. Honda, Y. Ogihara, S. Hashimoto, Y. Iwamoto, Thermal shock properties of porous alumina for support carrier of hydrogen membrane materials, Ceram. Eng. Sci. Proc., 31 (2010) 127–137.
[31] M.J. Cao, Y. Zhang, B.K. Zhang, Z.Q. Liu, X.S. Ma, C.M. Chen, The preparation of a modified PVDF hollow fiber membrane by coating with multiwalled carbon nanotubes for high antifouling performance, RSC Adv., 10 (2020) 1848–1857.
[32] S. Elmaleh, W. Naceur, Transport of water through an inorganic composite membrane, J. Membr. Sci., 66 (1992) 227–234.
[33] S.K. Hubadillah, M.H.D. Othman, A.F. Ismail, M.A. Rahman, J. Jaafar, Y. Iwamoto, S. Honda, M.I.H.M. Dzahir, M.Z.M. Yusop, Fabrication of low cost, green silica based ceramic hollow fibre membrane prepared from waste rice husk for water filtration application, Ceram. Int., 44 (2018) 10498–10509.
[34] M. Lee, B. Wang, Z.T. Wu, K. Li, Formation of micro-channels in ceramic membranes – spatial structure, simulation, and potential use in water treatment, J. Membr. Sci., 483 (2015) 1–14.
[35] N. Abdullah, N. Yusof, W.J. Lau, J. Jaafar, A.F. Ismail, Recent trends of heavy metal removal from water/wastewater by membrane technologies, J. Ind. Eng. Chem., 76 (2019) 17–38.
[36] S.R.H. Abadi, M.R. Sebzari, M. Hemati, F. Rekabdar, T. Mohammadi, Ceramic membrane performance in microfiltration of oily wastewater, Desalination, 265 (2011) 222–228.
[37] A.B.D. Aziz, M.H.D. Othman, N.A. Hashim, M.A. Rahman, J. Jaafar, S.K. Hubadillah, Z.S. Tai, Pretreated aluminium dross waste as a source of inexpensive alumina-spinel composite ceramic hollow fibre membrane for pretreatment of oily saline produced water, Ceram. Int., 45 (2019) 2069–2078.